Clinical Radiology 74 (2019) 406.e9–406.e18

Contents lists available at ScienceDirect

Clinical Radiology

journal homepage: www.clinicalradiologyonline.net

Differentiating between hepatocellular carcinoma and intrahepatic cholangiocarcinoma using contrast-enhanced MRI features: a systematic review and meta-analysis

M.-W. You [a], S.J. Yun [b,*]

[a] *Department of Radiology, Kyung Hee University Hospital, 23, Kyungheedae-ro, Dongdaemun-gu, Seoul 02447, Republic of Korea*

[b] *Department of Radiology, Kyung Hee University Hospital at Gangdong, Kyung Hee University School of Medicine, 892 Dongnam-ro, Gangdong-gu, Seoul 05278, Republic of Korea*

ARTICLE INFORMATION

Article history:
Received 31 August 2018
Accepted 27 December 2018

AIM: To identify magnetic resonance imaging (MRI) features for differentiating hepatocellular carcinoma (HCC) from intrahepatic cholangiocarcinoma (IHCC) and summarise their diagnostic accuracy.

MATERIALS AND METHODS: PubMed and EMBASE were searched for studies that employed MRI features to differentiate HCC from IHCC. Overlapping descriptors used to denote the same imaging finding in different studies were subsumed under a single feature. The pooled diagnostic accuracies, including the diagnostic odds ratios (DORs) and 95% confidence intervals (CIs) of the identified features, were calculated using a bivariate random-effects model.

RESULTS: In total, 1,370 patients with HCC and 687 patients with IHCC in 14 studies were included. Fifty-two descriptors were subsumed under 15 MRI features. Of these, 11 features were informative for differentiating HCC from IHCC. The five MRI features favouring HCC were capsule, arterial diffuse enhancement, portal venous washout, conventional washout, and intralesional fat; the six MRI features favouring IHCC were surface retraction, arterial rim enhancement, progressive enhancement, target appearance on diffusion-weighted and hepatobiliary phase (HBP) images, and bile duct dilatation. These features tended to show high specificity, but low sensitivity. Useful MRI features with high DORs (>20) were capsule (34; 95% CI, 5–215) and intralesional fat (23; 4–85) for HCC and arterial rim enhancement (31; 6–160), progressive enhancement (24; 8–73), and target appearance on HBP images (29; 3–261) for IHCC.

CONCLUSION: Eleven informative MRI features for differentiating HCC from IHCC were identified. These features will assist in the accurate diagnosis of these diseases and in disease outcome prediction.

* Guarantor and correspondent: S. J. Yun, Department of Radiology, Kyung Hee University Hospital at Gangdong, Kyung Hee University School of Medicine, 892 Dongnam-ro, Gangdong-gu, Seoul, 05278, Republic of Korea. Tel.: +82 2 440 693; fax: +82 2 440 6932.
E-mail address: zoomknight@naver.com (S.J. Yun).

https://doi.org/10.1016/j.crad.2018.12.016
0009-9260/

Introduction

Hepatocellular carcinoma (HCC) is the most common primary hepatic malignancy, followed by intrahepatic cholangiocarcinoma (IHCC); the incidence of these two common malignant hepatic tumours, in parallel with their mortality, has markedly increased worldwide in recent years.[1,2] Well-known risk factors for HCC, such as cirrhosis and chronic hepatitis B and C, have also been revealed as important risk factors in the pathogenesis of IHCC.[3] Although IHCC and HCC share similar risk factors, the treatment options and prognoses differ significantly between the two; for HCC, various treatment options, including surgical resection, local ablative therapy, and liver transplantation, are available, whereas surgical resection with negative margins is the only curative treatment for IHCC.[4] Therefore, accurate differentiation of IHCC and HCC is an important clinical issue.

The diagnosis of HCC can be made non-invasively by using imaging diagnostic criteria, one example of which is the Liver Imaging–Reporting and Data System (LI-RADS).[5] In LI-RADS, categories reflecting the relative probability of HCC are assigned to liver observations based on the presence of major and ancillary imaging features. The five major imaging features are arterial hyperenhancement, washout appearance, enhancing capsule, size, and threshold growth.[6] Although IHCC usually shows an enhancement pattern that is distinct from that of HCC, including arterial hypovascularity and the lack of delayed washout, arterial enhancement in IHCC has often been encountered in clinical practice, making its differentiation from HCC challenging.[1,4]

Additionally, in magnetic resonance imaging (MRI) with hepatobiliary agents (HBAs), the presence of washout appearance may be ambiguous due to parenchymal uptake of the liver starting from 3–5 minutes.[7] Hence, true delayed washout can be more easily assessed with extracellular contrast agents (ECAs) than with HBAs, as noted in a previous computed tomography study.[8]

Although a variety of studies have investigated the utility of MRI features for differentiating between HCC and IHCC, a comprehensive analysis of the distinct imaging findings for each tumour and their diagnostic performance needs to be conducted to improve the precision with which these tumours can be differentiated. Therefore, the present meta-analysis was undertaken to clearly identify the distinctive imaging features for HCC and IHCC, including their diagnostic ability, to provide straightforward guidance for differentiating between HCC and IHCC.

Materials and methods

This meta-analysis followed the guidelines of the Preferred Reporting Items for a Systematic Review and Meta-analysis of Diagnostic Test Accuracy Studies (PRISMA-DTA) statement.[9]

Literature search strategy

A computerised search of PubMed and studies captured in only the EMBASE databases was performed to identify relevant original literature concerning the diagnostic performance of MRI features for differentiating between HCC and IHCC (through 31 July 2018). Search terms related to "hepatocellular carcinoma" or "cholangiocarcinoma" were combined with "magnetic resonance imaging" as follows: ([cholangiocarcinoma] OR ["IHCC"]) AND ([hepatocellular carcinoma] OR [hepatoma] OR ["HCC"]) AND ([magnetic resonance imaging] OR [MR imaging] OR ["MRI"]) AND ([accuracy] OR [sensitivity] OR [specificity] OR [comparison] OR [comparing] OR [comparative] OR [differentiation] OR [differentiated] OR [distinguishing]). The bibliographies of identified articles were screened to determine additional relevant studies. The search was limited to studies in English; however, there were no restrictions regarding the publication date, species, or study setting. Two investigators (M.-W.Y. and S.J.Y.) screened the titles and abstracts for potential eligibility and disagreements were resolved by discussion.

Inclusion criteria

Studies (or subsets of studies) that investigated the performance of MRI features were eligible for inclusion. The inclusion criteria were as follows: population, original studies that included patients with HCC and IHCC who underwent contrast-enhanced MRI; reference standard, histopathologically confirmed HCC or IHCC; study design, observational studies (retrospective or prospective); and outcomes, availability of sufficient information to reconstruct 2×2 contingency tables for the sensitivity and specificity of MRI features for differentiating between HCC and IHCC.

Exclusion criteria

The exclusion criteria were as follows: case reports and series; review articles, editorials, letters, comments, and conference proceedings; studies not pertaining to the field of interest; studies with insufficient data for reconstructing 2×2 tables; studies with combined HCC and IHCC; and studies with overlapping patients and data. When an overlapping study population was found, the study with the largest study population was included.

Data extraction

The following data were extracted using standardised data forms: demographic and clinical characteristics of the patients, including the mean age, sex, patient numbers, and patient population; study characteristics, including the authors, publication years, patient recruitment durations, study design, reference standard, and blinding to the reference standard; MRI characteristics, including the scanner type, technical parameters, and interpretations; and the diagnostic performance of MRI features, which was

based on a 2 × 2 table showing the number of true-positive, false-positive, false-negative, and true-negative results. If two or more reviewers independently assessed the diagnostic accuracy, the result with the highest accuracy was extracted. One reviewer (M.-W.Y.) extracted the data, and a second reviewer (S.J.Y.) double-checked the accuracy of the extracted data.

Quality assessment

The methodological quality of the included studies was independently assessed by two reviewers (M.-W.Y. and S.J.Y.) using tailored questionnaires and criteria provided by the Quality Assessment of Diagnostic Accuracy Studies-2 (QUADAS-2).[10] Any disagreement was resolved in consensus.

Data synthesis and analyses

Patient demographic characteristics and extracted covariates were summarised using standard descriptive statistics. Continuous variables are expressed as means and 95% confidence intervals (CIs), while categorical variables are expressed as frequencies or percentages, unless stated otherwise.

A bivariate random-effects model was used for analysing and pooling the diagnostic performance measures (sensitivity and specificity) for identified MRI features. To derive summary estimates of the diagnostic performance of each feature, estimates of the observed sensitivities and specificities were plotted in forest plots and hierarchical summary receiver operating characteristic (HSROC) curves derived from individual study results. These results were plotted using HSROC curves with 95% CIs and prediction regions. In addition, pooled sensitivities, specificities, diagnostic odds ratios (DORs), areas under the curve, and positive and negative likelihood ratios (LRs) were calculated. Features with a pooled DOR whose 95% CI did not include 1 were considered informative.[11–13] If a feature was analysed in less than four studies or it was not clearly defined, data pooling was not performed.

Heterogeneity among the studies was determined using the I^2 inconsistency index (0–40%, might not be important; 30–60%, might represent moderate heterogeneity; 50–90%, might represent substantial heterogeneity; and 75–100%, represents considerable heterogeneity).[14] When heterogeneity was noted, its "threshold effect" was analysed by visually assessing the coupled forest plots of the sensitivity and specificity. A meta-analysis of the diagnostic test accuracy was performed to simultaneously evaluate a pair of outcomes (i.e., sensitivity and specificity). Sensitivity and specificity are commonly inversely correlated and influenced by a threshold (cut-off value). Moreover, the correlation between the sensitivity and false-positive rate was assessed using Spearman's correlation coefficient; a coefficient that was >0.6 was considered to indicate a considerable threshold effect.[15]

When ≥10 studies for MRI features were included, a meta-regression analysis was performed to further explore the reasons for heterogeneity by including covariates in the bivariate model. When <10 studies for MRI features were included, a meta-regression analysis could not be performed because most of the results were not available due to computation failure. The following covariates were considered: enrolment, total number of patients, size of HCC, size of IHCC, contrast agent, condition of the liver background, and consensus. Deeks' funnel plots[16] of individual studies were omitted to evaluate publication bias according to the PRISMA-DTA. The Midas and Metandi modules in Stata version 10.0 (StataCorp, College Station, TX) and R version 3.0.2 (R Foundation for Statistical Computing, Vienna, Austria) with the Mada package were used to perform the statistical analyses.

Results

Literature search

Fig 1 shows a flow diagram summarising the literature search. During the initial search, 595 studies were identified. After removing 90 duplicates, 505 titles and abstracts were reviewed and 477 studies excluded for the following reasons: case reports/letters/editorials/conference abstracts (n=124), review articles/guidelines/consensus statements (n=146), and not related to the field of interest (n=207). After reviewing the full text of 28 eligible articles, 14 were excluded for the following reasons: insufficient data for 2 × 2 table reconstruction (n=4),[17–20] focus on the diagnostic performance of MRI features of combined HCC-IHCC (n=5),[21–25] and partially overlapping study populations (n=5).[2,26–29] Finally, 14 studies[30–43] evaluating the diagnostic performance of MRI features for differentiating between HCC and IHCC were included.

Study and patient characteristics

In total, 1,370 patients with HCC and 687 patients with IHCC were included. One study[42] did not document the total

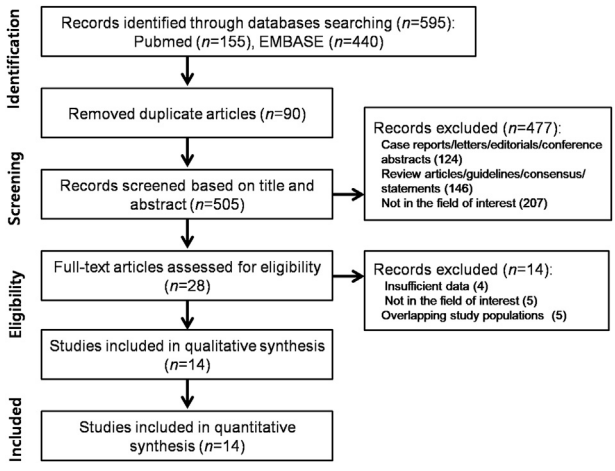

Figure 1 Flow diagram showing the study selection process for the meta-analysis.

patient number. The proportion of HCCs was 44.4–89.6%. The ranges of mean ages of the patients with HCC and IHCC were 46–69.9 years and 55–68.3 years, respectively (Table 1). Six studies[31,32,35,41–43] enrolled only patients with chronic liver disease, including cirrhosis, and eight studies[30,33,34,36–40] enrolled the patients heterogeneously (normal liver and chronic liver disease, including cirrhosis).

The study design was prospective in two studies[35,38] and retrospective in 12.[30–34,36,37,39–43] Eleven studies[30,32–41] involved consecutive patient enrolment, whereas three[31,42,43] involved non-consecutive enrolment. All studies used histopathological findings as the reference standard (Table 2).

The MRI characteristics are summarised in Table 3. Three studies[31,33,40] used 3 T MRI systems, seven[31,34,36–38,40,41] used 1.5 T systems, and four[30,34,36,43] used a 1.5 or 3 T systems. All studies used gadolinium-based contrast agents, with gadoxetic acid being the most common. The section thickness ranged from 2 to 5 mm, and it was not reported in one study.[43]

Categorisation of MRI features

There were 74 overlapping descriptors in the 14 studies. Of these, 22 were excluded from the meta-analysis because they referred to MRI features that were investigated in less than four studies. Finally, 52 descriptors were subsumed under the following 15 MRI features: capsule, arterial diffuse enhancement, portal venous washout, conventional washout (washout in the delayed phase [DP] of ECA-MR images and in the transitional phase [TP] of HBA-MR images), wash in and out, intralesional fat, portal vein thrombosis, lobulate shape, capsular retraction, arterial rim enhancement, progressive enhancement, persistent enhancement, target appearance on diffusion-weighted (DW) images, target appearance on hepatobiliary phase (HBP) images, and bile duct dilatation. These were included in the meta-analysis. Fig 2 is a flow diagram showing the MRI feature categorisation.

Study quality

The quality of the included studies, as assessed by the QUADAS-2 tool, was moderate or excellent, with all studies satisfying at least five of the seven items (Fig 3). With regard to patient selection, three studies[31,42,43] were considered to have a high risk of bias because they were case–control studies with non-consecutive enrolment. As for the index test and reference standard, all studies[30–43] were considered to have a low risk of bias because they were conducted after blinding from the reference standard and used histopathological findings as a reference standard. With regard to flow and timing, an unclear bias risk was considered for the 10 studies[30,31,33–35,37,38,41–43] that did not report the time interval between MRI and the reference standard. All studies, except three,[31,35,37] had low applicability with respect to patient selection because they included only patients with tumours of a specific size (≤3 cm) or patients with specific histological (scirrhous or diffuse) HCC.

Table 1
Characteristics of the subjects.

First author (ref)	No. of total patients	No. of total lesions	Liver background	HCC			IHCC		
				Mean age, yrs (range)	Male:female	Mean size, cm (range)	Mean age, yrs (range)	Male:female	Mean size, cm (range)
Choi[32]	144	165	CLD (cirrhosis)	58 (37–75)	61:11	4.2 (1–19.8)	55 (36–85)	56:16	3 (1–20)
Choi[33]	216	216	Normal/CLD	53.1 (24–76)	69:27	4.0 (1.2–15.5)	62.1 (36–81)	79:41	5.2 (1.5–14)
Huang[35]	683	683	CLD (cirrhosis)	46 (23–82)	500:112	2.4 (0.7–3.0)	55 (29–77)	51:20	2.3 (0.6–3.0)
Kim[36]	104	104	Normal/CLD	57.3	46:12	NR	62.3	29:17	NR
Lin[38]	19	19	Normal/CLD	NR	NR	NR	NR	NR	NR
Park[40]	82	82	Normal/CLD	53.9 (25–74)	28:13	4.9 (1.5–12.0)	62.3 (40–79)	25:16	4.7 (1.8–9.7)
Piscaglia[41]	39	47	CLD (cirrhosis)	NR	NR	NR	65.42 (52–77)	11:2	3 (1.5–8.5)
Wengert[43]	64	64	CLD (cirrhosis)	NR	NR	5 (1–15)	NR	NR	6 (2–20)
Asayama[30]	36	36	Normal/CLD	58.5	18:4	7.5 (2.0–16.5)	62.4	10:4	5 (1.5–7.5)
Chen[31]	44	44	CLD (cirrhosis)	56.91 (34–67)	16:6	5.305 (1.5–13.1)	58.32 (31–69)	16:6	8.177
Haradome[34]	74	74	Normal/CLD	69.9 (33–84)	37:14	3.76	68.3 (45–81)	17:6	3.03
Kim[37]	61	61	Normal/CLD	NR	NR	12 (6–21)	NR	NR	9.9 (6–18)
Quaia[42]	NR	76	CLD (cirrhosis)	NR	NR	4.76 (1–12)	NR	NR	5.06 (2–12)
Ni[39]	395	395	Normal/CLD	55.0 (28–80)	183:32	5.1 (1.8–8.4)	60.0 (28–80)	115:65	5.7 (2.8–8.6)

No., number; CLD, chronic liver disease; HCC, hepatocellular carcinoma; IHCC, intrahepatic cholangiocarcinoma; yrs, years; NR, not reported.

Table 2
Characteristics of the studies.

First author (ref)	Year	Locale	Study period	Study design	Reference standard	Blinding from reference standard
Choi[32]	2017	South Korea	2008.1–2014.9	Retrospective, consecutive	Histopathology	Blinding
Choi[33]	2018	South Korea	2010.1–2016.10	Retrospective, consecutive	Histopathology	Blinding
Huang[35]	2016	China	2009.10–2014.12	Prospective, consecutive	Histopathology	Blinding
Kim[36]	2016	South Korea	2011.11–2013.11	Retrospective, consecutive	Histopathology	Blinding
Lin[38]	2016	Taiwan	2014.1–2015.9	Prospective, consecutive	Histopathology	Blinding
Park[40]	2013	South Korea	2010.1–2012.6	Retrospective, consecutive	Histopathology	Blinding
Piscaglia[41]	2015	Italy	2008–2013	Retrospective, consecutive	Histopathology	Blinding
Wengert[43]	2017	Austria	2001.1–2013.12	Retrospective, non-consecutive	Histopathology	Blinding
Asayama[30]	2015	Japan	2008.6–2011.5	Retrospective, consecutive	Histopathology	Blinding
Chen[31]	2017	China	2010.1–2015.12	Retrospective, non-consecutive	Histopathology	Blinding
Haradome[34]	2017	Japan	2009.1–2016.6	Retrospective, consecutive	Histopathology	Blinding
Kim[37]	2009	South Korea	2004.1–2007.4	Retrospective, consecutive	Histopathology	Blinding
Quaia[42]	2015	Italy	2009.11–2013.11	Retrospective, non-consecutive	Histopathology	Blinding
Ni[39]	2018	China	2009.1–2015.10	Retrospective, consecutive	Histopathology	Blinding

Table 3
Magnetic resonance imaging (MRI) characteristics.

First author (ref)	Scanner			Technical parameters			Interpretation	
	Vendor	Model	Magnet strength (T)	Contrast	Sequences	Minimum ST (mm)	No. of readers	Reader experience (yrs)
Choi[32]	Siemens	Avanto	1.5	Gadoxetic acid	T1WI, T2WI, T1DCE (AP, PVP, TP, HBP)	4	2, independent	12/6
Choi[33]	Philips	Achieva	3.0	Gadoxetic acid	T1W IP-OP, T2WI, DWI, T1DCE (AP, PVP, TP, HBP)	2	2, independent	16/10
Huang[35]	GE	Signa Optima	1.5	Gadopentetate dimeglumine	T1WI, T2WI, T1DCE (AP, PVP, DP)	5	2, independent	30/10
Kim[36]	GE, Philips, Siemens	Signa HDxt/ Ingenia/ Magnetom Verio	1.5/3.0	Gadoxetic acid	T1W IP-OP, T2WI, DWI, T1CE (AP, PVP, TP, HBP)	3	2, consensus	11/8
Lin[38]	GE	Discovery	1.5	Gadopentetate dimeglumine	NR except T1DCE	5	1	6
Park[40]	Philips	Achieva	3.0	Gadoxetic acid	T1W IP-OP, T2WI, DWI, T1DCE (AP, PVP, TP, HBP)	2	2, consensus	13/5
Piscaglia[41]	GE, Siemens	Signa/Avanto	1.5	Gadoxetic acid	T1W IP-OP, T2WI, T1DCE (AP, PVP, TP, HBP)	2	2, independent	NR
Wengert[43]	Siemens, Philips	NR	1.5/3.0	Gadoterate meglumine/gadovist/ gadoxetic acid	T1W IP-OP, T2WI, DWI, T1DCE (AP, PVP, DP, HBP)	NR	4, independent	20/5/4/3
Asayama[30]	Philips	Intera Achieva/ Achieva	1.5/3.0	Gadoxetic acid	T1W IP-OP, T2WI, DWI, T1DCE (AP, PVP, TP, HBP)	3	2, consensus	17/16
Chen[31]	GE	Signa/Discovery 750	3.0	Gadodiamide	T1WI, T2WI, DWI, T1DCE (AP, PVP, TP, HBP)	4	2, independent	25/5
Haradome[34]	NR	NR	1.5/3.0	Gadoxetic acid	T1WI, T2WI, DWI, T1DCE (AP, PVP, TP, HBP)	3.8	2, consensus	20/9
Kim[37]	Siemens	Magnetom Symphony	1.5	Gadopentetate dimeglumine with ferucarbotran	T1W IP-OP, T2WI, T1DCE (AP, PVP, TP, HBP)	3.5	2, consensus	At least 5
Quaia[42]	Philips	Achieva	1.5	Gadobenate dimeglumine	T1WI, T2WI, T1DCE (AP, PVP, TP, HBP)	5	2, consensus	10/8
Ni[39]	Siemens	Avanto	1.5	Gadopentetate dimeglumine	T1WI, T2WI, DWI, T1DCE (AP, PVP, DP)	5	2, consensus	NR

No., number; WI, weighted imaging; DCE, dynamic contrast-enhanced; AP, arterial phase; PVP, portal venous phase; TP, transitional phase; HBP, hepatobiliary phase; DP, delayed phase; IP, in-phase; OP, opposed-phase; DWI, diffusion-weighted imaging; ST, slice thickness; NR, not reported; yrs, years.

Overall diagnostic accuracy

The pooled sensitivities and specificities for the 15 MRI features (seven MRI features favouring HCC and eight MRI features favouring IHCC) are presented in Table 4, along with the pooled areas under the curve, pooled DORs, pooled positive LRs, and pooled negative LRs. There was a general tendency for these features, except for conventional washout, to show relatively high specificity but low sensitivity. Based on the pooled DORs with 95% CIs, 11 of the 15 MRI features (five MRI features favouring HCC and six MRI features favouring IHCC) were informative for

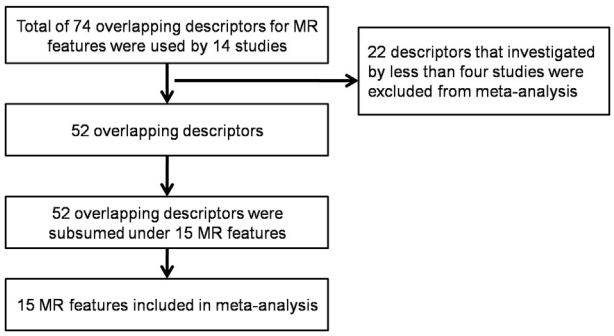

Figure 2 Flow diagram showing the process of MRI feature categorisation.

differentiating between HCC and IHCC, while four MRI features (wash in and out, portal vein thrombosis, lobulate shape, persistent enhancement) were not informative. Among the five MRI features favouring HCC, the pooled DORs of capsule (DOR, 34; 95% CI, 5–215) and intralesional fat (DOR, 23; 95% CI, 4–85) were >20. Forest plots and HSROC curves of the capsule and intralesional fat features are shown in Fig 4a,b. Among the six MRI features favouring IHCC, the pooled DORs of arterial rim enhancement (DOR, 31; 95% CI, 6–160), target appearance on HBP images (DOR, 29; 95% CI, 3–261), and progressive enhancement (DOR, 24; 95% CI, 8–73) were >20. Forest plots and HSROC curves of the arterial rim enhancement, target appearance on HBP images, and progressive enhancement features are shown in Fig 4c–e. Data for the other 10 informative MRI features are presented in the Electronic Supplementary Materials, Fig S1a–j.

Considerable heterogeneity was present for all features except bile duct dilatation; however, no threshold effect was identified (correlation coefficient, −0.263 to 0.585).

Meta-regression analysis

The source of heterogeneity in terms of specificity was the liver background. Specifically, studies with only chronic liver disease showed significantly higher specificity than did those with heterogeneous liver backgrounds. The source of heterogeneity in terms of sensitivity was not identified (Table 5).

Discussion

In this meta-analysis, the diagnostic performance of commonly used informative MRI features favouring a diagnosis of HCC or IHCC were analysed. The five useful MRI features favouring HCC were arterial diffuse enhancement, portal venous washout, conventional washout (DP on ECA-MR images, TP on HBA-MR images), capsule, and intralesional fat. Four of these five MRI features are consistent with the major features of HCC in LI-RADS, except for intralesional fat. According to present study, intralesional fat showed the highest DOR among the five useful MRI features favouring HCC, which corresponds to the "fat in mass" ancillary feature in LI-RADS. The intralesional fat feature revealed the highest specificity (97%), but very low sensitivity (32%), indicating that using this feature alone can yield many false negatives. Furthermore, this feature cannot be applied to every case of HCC, because a considerable number of HCCs do not contain a fat component. This might explain why this feature is not included as a major feature for diagnosing HCC in LI-RADS.

Another feature with a high DOR was capsule, and this feature is a major feature in LI-RADS. In the latest version of LI-RADS, however, capsule has been revised to enhancing capsule.[44] Among the seven studies, the evaluated capsular appearance was analysed. The capsule in four studies corresponded to the definition of enhancing capsule, whereas the other three studies did not explain the definition of capsule in their reports.

As mentioned above, washout appearance can be more easily evaluated with ECA-MRI than with HBA-MRI according to a previous study.[8] With HBA-MRI, the "pseudo washout" on TP images may be confusing, and therefore several studies have focused on the comparison between

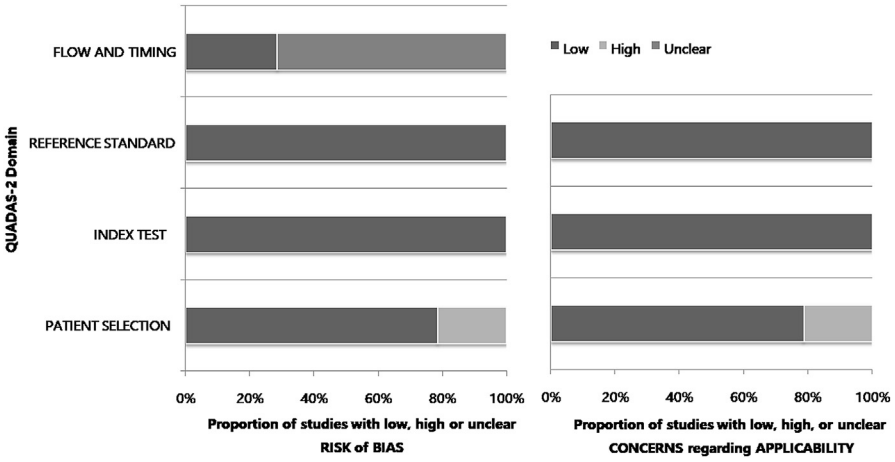

Figure 3 Grouped bar charts showing the risk of bias (left) and concern for applicability (right) of the 14 included studies, using the Quality Assessment of Diagnostic Accuracy Studies-2 (QUADAS-2) domains.

portal venous washout and conventional washout on HBA-MRI images to diagnose HCC.[32,36] In the present meta-analysis, portal venous washout and conventional washout had similar pooled DORs. The specificity of portal venous washout was slightly higher than that of conventional washout, but at the expense of slightly lower sensitivity. As such, both portal venous washout and conventional washout need to be considered to consolidate an accurate imaging diagnosis of HCC in clinical practice.

Herein, there was a general tendency of MRI features favouring IHCC to show higher specificity but lower sensitivity. The radiological diagnosis of IHCC can be made by adding multiple specific MRI features to decrease the false-negative rate, because unlike HCC, IHCC does not have sensitive imaging features. Several studies have demonstrated that IHCC shows arterial enhancement, especially small IHCCs measuring <3 cm, and thus this feature overlaps with that of HCC[1,4,35]; however, the pattern of arterial enhancement in IHCC differs from that of HCC. In this meta-analysis, arterial rim enhancement was the most useful MRI feature of IHCC with the highest DOR, while progressive enhancement and target appearance on HBP images were useful features with moderate DORs.

Progressive enhancement can be more clearly assessed with ECA-MRI than HBA-MRI similar to washout appearance, as ECA-MRI mainly evaluates haemodynamic change of tumours.[45] In this study, eight studies evaluated progressive enhancement, half of the studies used ECA-MRI whereas the other half used HBA-MRI.

Among the six useful MRI features favouring IHCC, four features (arterial rim enhancement, progressive delayed enhancement, target appearance on DW and HBP images) were consistent with a targetoid appearance in LI-RADS, corresponding to the LR-M category; however, other tumours, such as HCC with atypical features and combined HCC–IHCC tumours, can be included in the LR-M category and show a targetoid appearance. That said, an imaging diagnosis pointing towards HCC (LR-5) or IHCC (LR-M) might have more prognostic value than an actual pathological diagnosis,[46] i.e., among the same combined HCC–IHCC tumours, tumours with imaging features favouring HCC would have a better prognosis, whereas tumours with imaging features favouring IHCC would have a worse prognosis. Thus, being aware of the informative MRI features favouring HCC and IHCC is helpful not only for ensuring a correct diagnosis but also for estimating the disease outcomes.

The present study has several limitations. First, a relatively small number of studies were included. Several studies were excluded because the sensitivities and specificities could not be calculated. Second, as suggested earlier, methodological differences were observed in the included studies, which were heterogeneous with respect to the design and total patient numbers. Although the statistical analysis of heterogeneity with regard to effect sizes indicated homogeneity among the studies, the methodological diversity may have contributed to the misinterpretation of the pooled estimates. Inevitably, relevant data for each

Table 4
The pooled sensitivity, specificity, diagnostic odds ratio, area under the curve, likelihood ratio, and threshold effect of individual MRI features.

MRI features	No. of studies	Sensitivity, %	Specificity, %	DOR	Pooled area under the curve	Pooled positive LR	Pooled negative LR	Threshold effect
Favouring HCC								
Capsule	7	58 (42–73)	96 (81–99)	34 (5–215)	0.84 (0.80–0.87)	15.0 (2.7–81.8)	0.44 (0.29–0.64)	0.034 (-0.738–0.767)
Arterial diffuse enhancement	7	81 (57–93)	80 (63–90)	18 (6–53)	0.87 (0.84–0.90)	4.1 (2.2–7.6)	0.23 (0.10–0.57)	0.507 (-0.308–0.893)
Portal venous washout	6	76 (58–88)	81 (51–94)	13 (3–64)	0.84 (0.80–0.87)	3.9 (1.3–11.9)	0.30 (0.15–0.58)	0.070 (-0.786–0.834)
Conventional washout	8	80 (64–90)	79 (70–87)	13 (5–39)	0.86 (0.82–0.89)	3.9 (2.5–6.1)	0.25 (0.13–0.50)	-0.068 (-0.781–0.722)
Wash in and out	4	80 (75–85)	86 (78–91)	7 (1–88)	0.87 (0.84–0.90)	5.7 (3.7–8.9)	0.23 (0.18–0.29)	0.585 (-0.615–0.968)
Intralesional fat	7	32 (13–59)	97 (91–99)	23 (4–85)	0.95 (0.93–0.97)	11.5 (3.6–36.6)	0.70 (0.49–1.00)	0.497 (-0.528–0.932)
Portal vein thrombosis	4	32 (6–77)	90 (79–95)	4 (1–23)	0.85 (0.82–0.88)	3.1 (0.9–10.2)	0.76 (0.42–1.37)	0.230 (-0.939–0.975)
Favouring IHCC								
Lobulate shape	7	55 (39–70)	82 (60–93)	6 (1–21)	0.71 (0.67–0.75)	3.1 (1.2–8.3)	0.55 (0.36–0.83)	0.127 (-0.634–0.763)
Capsular retraction	7	26 (19–34)	95 (88–98)	6 (3–14)	0.56 (0.52–0.61)	4.8 (2.2–10.3)	0.78 (0.71–0.87)	0.226 (-0.635–0.837)
Arterial rim enhancement	11	66 (48–80)	93 (72–99)	31 (6–160)	0.84 (0.81–0.87)	11.1 (2.2–56.8)	0.36 (0.23–0.56)	0.355 (-0.311–0.787)
Progressive enhancement	8	48 (24–73)	96 (91–99)	24 (8–73)	0.93 (0.90–0.95)	12.9 (5.4–30.8)	0.54 (0.33–0.88)	0.463 (-0.290–0.862)
Persistent enhancement	5	24 (11–44)	98 (90–100)	10 (1–100)	0.80 (0.76–0.83)	10.8 (1.8–67.1)	0.78 (0.62–0.97)	-0.105 (-0.845–0.772)
Target appearance on DW images	6	62 (41–80)	91 (53–99)	17 (4–75)	0.79 (0.75–0.82)	7.0 (1.2–39.1)	0.41 (0.28–0.60)	0.474 (-0.034–0.592)
Target appearance on HBP images	6	65 (41–83)	87 (44–98)	29 (3–261)	0.79 (0.75–0.82)	4.9 (1.1–22.6)	0.40 (0.27–0.59)	0.408 (-0.011–0.578)
Bile duct dilatation	7	40 (29–51)	95 (92–97)	11 (5–26)	0.92 (0.89–0.94)	7.3 (3.9–13.7)	0.64 (0.53–0.75)	-0.263 (-0.848–0.611)

Data in parentheses are 95% confidence intervals. MRI, magnetic resonance imaging; HCC, hepatocellular carcinoma; IHCC, intrahepatic cholangiocarcinoma; DW, diffusion-weighted; HBP, hepatobiliary phase; No., number; DOR, diagnostic odds ratio; LR, likelihood ratio.

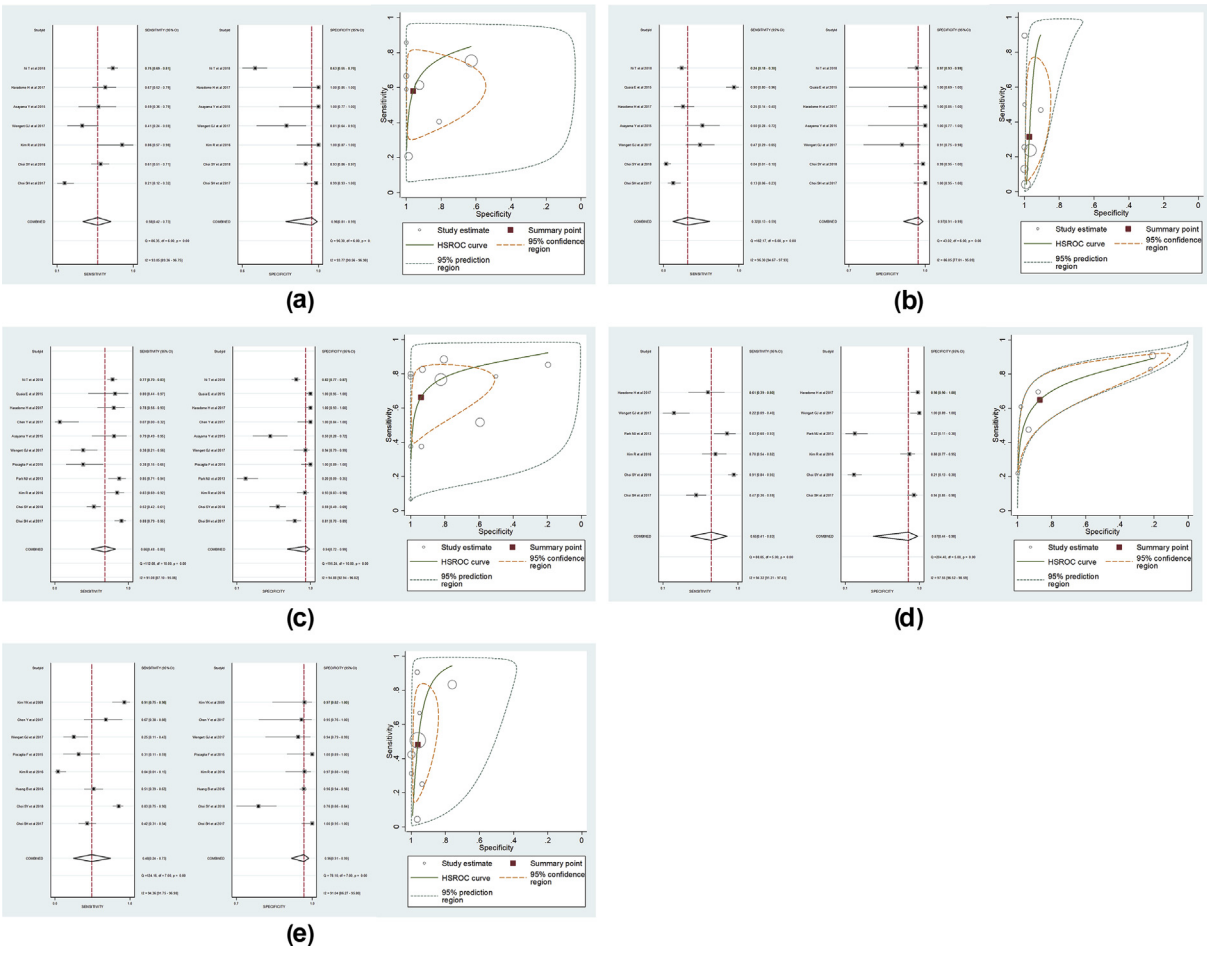

Figure 4 Coupled forest plots of the pooled sensitivity and specificity (left) and HSROC curves (right) show MRI features with informative pooled sensitivities and specificities with 95% confidence intervals. (a) Capsule. (b) Intralesional fat. (c) Arterial rim enhancement. (d) Target appearance on hepatobiliary phase (HBP) images. (e) Progressive enhancement.

Table 5
Results of the meta-regression analyses.

Covariate	No. of studies	Sensitivity (95% CI)	*p*-Value	Specificity (95% CI)	*p*-value
Arterial rim enhancement (n=11)					
Enrolment			0.06		0.31
Consecutive	8	0.75 (0.63–0.87)		0.86 (0.66–1.00)	
Non-consecutive	3	0.37 (0.09–0.64)		0.99 (0.98–1.00)	
No. of patients			0.36		0.77
≥100	4	0.77 (0.57–0.97)		0.82 (0.48–1.00)	
<100	6	0.55 (0.31–0.79)		0.95 (0.84–1.00)	
HCC size			0.10		0.11
≥5 cm	4	0.50 (0.22–0.78)		0.93 (0.75–1.00)	
<5 cm	5	0.78 (0.61–0.95)		0.90 (0.68–1.00)	
IHCC size			0.13		0.12
≥5 cm	6	0.53 (0.31–0.76)		0.95 (0.81–1.00)	
<5 cm	4	0.77 (0.57–0.96)		0.96 (0.82–1.00)	
Contrast agent			0.34		0.97
Gadoxetic acid	7	0.75 (0.59–0.91)		0.88 (0.65–1.00)	
Other gadolinium contrast agents	3	0.53 (0.19–0.86)		1.00 (0.97–1.00)	
Liver background			0.08		<0.01
Only chronic liver disease	5	0.51 (0.26–0.76)		0.99 (0.96–1.00)	
Heterogeneous	6	0.77 (0.61–0.92)		0.78 (0.49–1.00)	
Consensus			0.09		0.67
Yes	5	0.81 (0.68–0.93)		0.91 (0.71–1.00)	
No	6	0.46 (0.25–0.67)		0.97 (0.88–1.00)	

No., number; CI, confidence interval; HCC, hepatocellular carcinoma; IHCC, intrahepatic cholangiocarcinoma.

analytical level could not be retrieved from all studies. Third, there was some inconsistency in the terms used to indicate MRI features; for example, arterial nodular enhancement/arterial diffuse enhancement and peripheral hypointense rim on HBP images/target appearance on HBP images. The terms were standardised to more frequently used terms. Fourth, early HCCs are frequently hypovascular in the arterial phase.[47] In those cases, differentiation from IHCC is more difficult and non-invasive imaging diagnosis can be challenging. Finally, the diagnostic accuracy of various combinations of features was not assessed. In clinical practice, differentiating between HCC and IHCC relies on the combinations of various MRI features.

In conclusion, for HCC, arterial diffuse enhancement and conventional washout were the most sensitive features, whereas intralesional fat and capsule were the most useful features with high DORs. For IHCC, arterial rim enhancement, progressive enhancement, and target appearance on HBP images were the most useful features with high DORs. The information presented herein will assist not only in the accurate diagnosis of these diseases, but also in the prediction of disease outcomes.

Conflict of interest

There is no conflict of interest.

Appendix A. Supplementary data

Supplementary data to this article can be found online at https://doi.org/10.1016/j.crad.2018.12.016.

References

1. Kim SJ, Lee JM, Han JK, *et al*. Peripheral mass-forming cholangiocarcinoma in cirrhotic liver. *AJR Am J Roentgenol* 2007;**189**(6):1428–34.
2. Sheng RF, Zeng MS, Rao SX, *et al*. MRI of small intrahepatic mass-forming cholangiocarcinoma and atypical small hepatocellular carcinoma (</=3 cm) with cirrhosis and chronic viral hepatitis: a comparative study. *Clin Imag* 2014;**38**(3):265–72.
3. Palmer WC, Patel T. Are common factors involved in the pathogenesis of primary liver cancers? A meta-analysis of risk factors for intrahepatic cholangiocarcinoma. *J Hepatol* 2012;**57**(1):69–76.
4. Kim SA, Lee JM, Lee KB, *et al*. Intrahepatic mass-forming cholangiocarcinomas: enhancement patterns at multiphasic CT, with special emphasis on arterial enhancement pattern—correlation with clinicopathologic findings. *Radiology* 2011;**260**(1):148–57.
5. Mitchell DG, Bruix J, Sherman M, *et al*. LI-RADS (liver imaging reporting and data system): summary, discussion, and consensus of the LI-RADS management working group and future directions. *Hepatology (Baltimore, Md)* 2015;**61**(3):1056–65.
6. Tang A, Bashir MR, Corwin MT, *et al*. Evidence supporting LI-RADS major features for CT- and MR imaging-based diagnosis of hepatocellular carcinoma: a systematic review. *Radiology* 2018;**286**(1):29–48.
7. Joo I, Lee JM, Lee DH, *et al*. Noninvasive diagnosis of hepatocellular carcinoma on gadoxetic acid-enhanced MRI: can hypointensity on the hepatobiliary phase be used as an alternative to washout? *Eur Radiol* 2015;**25**(10):2859–68.
8. Furlan A, Marin D, Vanzulli A, *et al*. Hepatocellular carcinoma in cirrhotic patients at multidetector CT: hepatic venous phase versus delayed phase for the detection of tumour washout. *Br J Radiol* 2011;**84**(1001):403–12.
9. McInnes MDF, Moher D, Thombs BD, *et al*. Preferred reporting items for a systematic review and meta-analysis of diagnostic test accuracy studies: the PRISMA-DTA statement. *JAMA* 2018;**319**(4):388–96.
10. Whiting PF, Rutjes AW, Westwood ME, *et al*. QUADAS-2: a revised tool for the quality assessment of diagnostic accuracy studies. *Ann Intern Med* 2011;**155**(8):529–36.
11. Kim KW, Lee J, Choi SH, *et al*. Systematic review and meta-analysis of studies evaluating diagnostic test accuracy: a practical review for clinical researchers—part I. General guidance and tips. *Kor J Radiol* 2015;**16**(6):1175–87.
12. Lee J, Kim KW, Choi SH, *et al*. Systematic review and meta-analysis of studies evaluating diagnostic test accuracy: a practical review for clinical researchers—part II. Statistical methods of meta-analysis. *Kor J Radiol* 2015;**16**(6):1188–96.
13. Suh CH, Park SH. Successful publication of systematic review and meta-analysis of studies evaluating diagnostic test accuracy. *Kor J Radiol* 2016;**17**(1):5–6.
14. Higgins J, Green S. Cochrane handbook for systematic reviews of interventions. Version 5.1.0. The Cochrane Collaboration. Available at: http://handbook.cochrane.org/chapter_9/9_5_2_identifying_and_measuring_heterogeneity.htm. Accessed 1 August 2018.
15. Deville WL, Buntinx F, Bouter LM, *et al*. Conducting systematic reviews of diagnostic studies: didactic guidelines. *BMC Med Res Methodol* 2002;**2**:9.
16. Deeks JJ, Macaskill P, Irwig L. The performance of tests of publication bias and other sample size effects in systematic reviews of diagnostic test accuracy was assessed. *J Clin Epidemiol* 2005;**58**(9):882–93.
17. Choi SH, Kim SY, Lee SS, *et al*. Subtraction images of gadoxetic acid-enhanced MRI: effect on the diagnostic performance for focal hepatic lesions in patients at risk for hepatocellular carcinoma. *AJR Am J Roentgenol* 2017;**209**(3):584–91.
18. Park HJ, Jang KM, Kang TW, *et al*. Identification of imaging predictors discriminating different primary liver tumours in patients with chronic liver disease on gadoxetic acid-enhanced MRI: a classification tree analysis. *Eur Radiol* 2016;**26**(9):3102–11.
19. Peterson MS, Murakami T, Baron RL. MR imaging patterns of gadolinium retention within liver neoplasms. *Abdom Imag* 1998;**23**(6):592–9.
20. Rimola J, Forner A, Reig M, *et al*. Cholangiocarcinoma in cirrhosis: absence of contrast washout in delayed phases by magnetic resonance imaging avoids misdiagnosis of hepatocellular carcinoma. *Hepatology (Baltimore, Md)* 2009;**50**(3):791–8.
21. Fowler KJ, Sheybani A, Parker 3rd RA, *et al*. Combined hepatocellular and cholangiocarcinoma (biphenotypic) tumours: imaging features and diagnostic accuracy of contrast-enhanced CT and MRI. *AJR Am J Roentgenol* 2013;**201**(2):332–9.
22. Horvat N, Nikolovski I, Long N, *et al*. Imaging features of hepatocellular carcinoma compared to intrahepatic cholangiocarcinoma and combined tumour on MRI using liver imaging and data system (LI-RADS) version 2014. *Abdom Radiol (New York)* 2018;**43**(1):169–78.
23. Hwang J, Kim YK, Park MJ, *et al*. Differentiating combined hepatocellular and cholangiocarcinoma from mass-forming intrahepatic cholangiocarcinoma using gadoxetic acid-enhanced MRI. *J Magn Reson Imag* 2012;**36**(4):881–9.
24. Jeon TY, Kim SH, Lee WJ, *et al*. The value of gadobenate dimeglumine-enhanced hepatobiliary-phase MR imaging for the differentiation of scirrhous hepatocellular carcinoma and cholangiocarcinoma with or without hepatocellular carcinoma. *Abdom Imag* 2010;**35**(3):337–45.
25. Potretzke TA, Tan BR, Doyle MB, *et al*. Imaging features of biphenotypic primary liver carcinoma (hepatocholangiocarcinoma) and the potential to mimic hepatocellular carcinoma: LI-RADS analysis of CT and MRI features in 61 Cases. *AJR Am J Roentgenol* 2016;**207**(1):25–31.
26. Chong YS, Kim YK, Lee MW, *et al*. Differentiating mass-forming intrahepatic cholangiocarcinoma from atypical hepatocellular carcinoma using gadoxetic acid-enhanced MRI. *Clin Radiol* 2012;**67**(8):766–73.
27. Hwang J, Kim YK, Min JH, *et al*. Capsule, septum, and T2 hyperintense foci for differentiation between large hepatocellular carcinoma (>/=5 cm) and intrahepatic cholangiocarcinoma on gadoxetic acid MRI. *Eur Radiol* 2017;**27**(11):4581–90.
28. Min JH, Kim YK, Choi SY, *et al*. Differentiation between cholangiocarcinoma and hepatocellular carcinoma with target sign on diffusion-weighted imaging and hepatobiliary phase gadoxetic acid-enhanced MR imaging: classification tree analysis applying capsule and septum. *Eur J Radiol* 2017;**92**:1–10.

29. Park HJ, Kim YK, Park MJ, *et al*. Small intrahepatic mass-forming cholangiocarcinoma: target sign on diffusion-weighted imaging for differentiation from hepatocellular carcinoma. *Abdom Imag* 2013;**38**(4):793–801.
30. Asayama Y, Nishie A, Ishigami K, *et al*. Distinguishing intrahepatic cholangiocarcinoma from poorly differentiated hepatocellular carcinoma using precontrast and gadoxetic acid-enhanced MRI. *Diagn Interv Radiol (Ankara, Turkey)* 2015;**21**(2):96–104.
31. Chen Y, Pan Y, Shen KR, *et al*. Contrast-enhanced multiple-phase imaging features of intrahepatic mass-forming cholangiocarcinoma and hepatocellular carcinoma with cirrhosis: a comparative study. *Oncol Lett* 2017;**14**(4):4213–9.
32. Choi SH, Lee SS, Kim SY, *et al*. Intrahepatic cholangiocarcinoma in patients with cirrhosis: differentiation from hepatocellular carcinoma by using gadoxetic acid-enhanced MR imaging and dynamic CT. *Radiology* 2017;**282**(3):771–81.
33. Choi SY, Kim YK, Min JH, *et al*. Added value of ancillary imaging features for differentiating scirrhous hepatocellular carcinoma from intrahepatic cholangiocarcinoma on gadoxetic acid-enhanced MR imaging. *Eur Radiol* 2018 Jun;**28**(6):2549–60.
34. Haradome H, Unno T, Morisaka H, *et al*. Gadoxetic acid disodium-enhanced MR imaging of cholangiolocellular carcinoma of the liver: imaging characteristics and histopathological correlations. *Eur Radiol* 2017;**27**(11):4461–71.
35. Huang B, Wu L, Lu XY, *et al*. Small intrahepatic cholangiocarcinoma and hepatocellular carcinoma in cirrhotic livers may share similar enhancement patterns at multiphase dynamic MR imaging. *Radiology* 2016;**281**(1):150–7.
36. Kim R, Lee JM, Shin CI, *et al*. Differentiation of intrahepatic mass-forming cholangiocarcinoma from hepatocellular carcinoma on gadoxetic acid-enhanced liver MR imaging. *Eur Radiol* 2016;**26**(6):1808–17.
37. Kim YK, Han YM, Kim CS. Comparison of diffuse hepatocellular carcinoma and intrahepatic cholangiocarcinoma using sequentially acquired gadolinium-enhanced and Resovist-enhanced MRI. *Eur J Radiol* 2009;**70**(1):94–100.
38. Lin CC, Cheng YF, Chiang HJ, *et al*. Pharmacokinetic analysis of dynamic contrast-enhanced magnetic resonance imaging for distinguishing hepatocellular carcinoma from cholangiocarcinoma in pre-liver transplantation evaluation. *Transplant Proc* 2016;**48**(4):1041–4.
39. Ni T, Shang XS, Wang WT, *et al*. Different MR features for differentiation of intrahepatic mass-forming cholangiocarcinoma from hepatocellular carcinoma according to tumour size. *Br J Radiol* 2018;**91**(1088):20180017.
40. Park MJ, Kim YK, Park HJ, *et al*. Scirrhous hepatocellular carcinoma on gadoxetic acid-enhanced magnetic resonance imaging and diffusion-weighted imaging: emphasis on the differentiation of intrahepatic cholangiocarcinoma. *J Comp Assist Tomogr* 2013;**37**(6):872–81.
41. Piscaglia F, Iavarone M, Galassi M, *et al*. Cholangiocarcinoma in cirrhosis: value of hepatocyte specific magnetic resonance imaging. *Dig Dis* 2015;**33**(6):735–44.
42. Quaia E, Angileri R, Arban F, *et al*. Predictors of intrahepatic cholangiocarcinoma in cirrhotic patients scanned by gadobenate dimeglumine-enhanced magnetic resonance imaging: diagnostic accuracy and confidence. *Clin Imag* 2015;**39**(6):1032–8.
43. Wengert GJ, Baltzer PAT, Bickel H, *et al*. Differentiation of intrahepatic cholangiocellular carcinoma from hepatocellular carcinoma in the cirrhotic liver using contrast-enhanced MR imaging. *Acad Radiol* 2017;**24**(12):1491–500.
44. Elsayes KM, Hooker JC, Agrons MM, *et al*. 2017 Version of LI-RADS for CT and MR imaging: an update. *RadioGraphics* 2017;**37**(7):1994–2017.
45. Choi JY, Lee JM, Sirlin CB. CT and MR imaging diagnosis and staging of hepatocellular carcinoma: part II. Extracellular agents, hepatobiliary agents, and ancillary imaging features. *Radiology* 2014;**273**(1):30–50.
46. An C, Park S, Chung YE, *et al*. Curative resection of single primary hepatic malignancy: liver Imaging Reporting and Data System category LR-M portends a worse prognosis. *AJR Am J Roentgenol* 2017;**209**(3):576–83.
47. Takahashi M, Maruyama H, Shimada T, *et al*. Characterization of hepatic lesions (</= 30 mm) with liver-specific contrast agents: a comparison between ultrasound and magnetic resonance imaging. *Eur J Radiol* 2013;**82**(1):75–84.